Kinetics of a mixed spin-1 and spin-3/2 Ising system under a time-dependent oscillating magnetic field

Mustafa Keskin,[1] Ersin Kantar,[2] and Osman Canko[1]
[1]*Department of Physics, Erciyes University, 38039 Kayseri, Turkey*
[2]*Institute of Science, Erciyes University, 38039 Kayseri, Turkey*
(Received 1 February 2008; published 28 May 2008)

We present a study, within a mean-field approach, of the kinetics of the mixed spin-1 and spin-3/2 Ising model Hamiltonian with bilinear and biquadratic nearest-neighbor exchange interactions and a single-ion potential or crystal-field interaction in the presence of a time-dependent oscillating external magnetic field. We employ the Glauber transition rates to construct the mean-field dynamical equations. We investigate the time dependence of average magnetizations and the quadrupole moments, and the thermal behavior of the dynamic order parameters. From these studies, we obtain the dynamic phase transition (DPT) points and construct the phase diagrams in three different planes. Phase diagrams contain disordered (d), ferrimagnetic (i), the antiquadrupolar or staggered (a) phases, and four coexistence or mixed phase regions, namely, the $i+d$, $i+a$, $i+a+d$, and $a+d$, that strongly depend on interaction parameters. The system also exhibits the dynamic tricritical behavior in most cases, the reentrant behavior in few cases.

DOI: 10.1103/PhysRevE.77.051130 PACS number(s): 05.50.+q, 05.70.Fh, 64.60.Ht, 75.10.Hk

I. INTRODUCTION

Ferrimagnetic materials are currently the subject of a great deal of interest due to the their possible useful properties for technological applications as well as academic researches. Mixed-spin Ising systems provide good models to investigate ferrimagnetism. One of the earliest, simplest and as well as most extensively studied mixed spin Ising models is the spin-1/2 and spin-1 mixed system. Equilibrium behavior of this system has been extensively studied by the well-known method in the equilibrium statistical physics (see [1–5] and references therein). Few works have been done for investigating the nonequilibrium properties of the system [6–8].

The spin-1 and spin-3/2 mixed system has received less attention. However, this system was used to study iron nitride compounds, specifically the Monte Carlo (MC) simulations were applied to study of a mixed spin-1 and spin-3/2 Ising model to investigate a characteristic feature of Fe_4N [9]. The equilibrium properties of the mixed spin-1 and spin-3/2 Ising system were examined by various methods such as the effective-field theory (EFT) [10], mean-field approximation (MFA) based on Bogoliubov inequality for the Gibbs free energy [11], the cluster variation method with the pair approximation (CVMPA) [12], and the MC simulations [9,13]. The exact formulation of the mixed spin-1 and spin-3/2 Ising ferrimagnetic systems on the Bethe lattice using the exact recursion equations was given in detail [14].

While equilibrium properties of the mixed spin-1 and spin-3/2 Ising systems have been studied by various methods, to our knowledge the nonequilibrium properties of the systems have not been investigated. Therefore, in this work we are going to investigate dynamical aspect of the mixed spin-1 and spin-3/2 Ising ferromagnetic model Hamiltonian with bilinear and biquadratic nearest-neighbor exchange interactions and a single-ion potential or crystal-field interaction in the presence of a time-dependent oscillating external magnetic field. We use the Glauber-type stochastic dynamics [15] to describe the time evolution of the system and obtain the mean-field dynamical equations. The nature (continuous and discontinuous) of transition is characterized by studying the thermal behaviors of dynamic order parameters. The dynamic phase transition (DPT) points are obtained and the dynamic phase diagrams are presented in three different planes.

The organization of the remaining part of this paper is as follows. In Sec. II, the model and its formulations, namely, the derivation of the set of mean-field dynamic equations, are given by using Glauber-type stochastic dynamics in the presence of a time-dependent oscillating external magnetic field. In Sec. III, the numerical results for average order parameters, the DPT points and phase diagrams are studied in detail. Finally, we give a summary and conclusion in Sec. IV.

II. MODEL AND FORMULATIONS

The mixed spin-1 and spin-3/2 Ising model is described as a two-sublattice system, with spin variables $\sigma_i = \pm 1, 0$ and $S_i = \pm 3/2, \pm 1/2$ on the sites of sublattices A and B, respectively. The system has four long-range order parameters which are introduced as follows: Two average magnetizations $\langle \sigma \rangle$ and $\langle S \rangle$ for the A and B sublattices, respectively, which are the excess of one orientation over the other, also called the dipole moments. Two average quadrupole moments, $\langle q_A \rangle$, which is a linear function of average square magnetization, i.e., $\langle 3\sigma_i^2 - 2 \rangle$, only for the A sublattice, and $\langle q_B \rangle$, which is a linear function of average square magnetization, $\langle S_i^2 - 5/4 \rangle$, only for the B sublattice.

The mixed spin-1 and spin-3/2 Ising model Hamiltonian with bilinear (J) and biquadratic (K) nearest-neighbor exchange interactions and a single-ion potential or crystal-field interaction (D) in the presence of a time-dependent oscillating external magnetic field is

$$\mathcal{H} = -J\sum_{\langle ij\rangle}\sigma_i^A S_j^B - K\sum_{\langle ij\rangle}[3(\sigma_i^A)^2-2][(S_j^B)^2-5/4] - D\left(\sum_i[3(\sigma_i^A)^2-2]+\sum_j[(S_j^B)^2-5/4]\right) - H\left(\sum_i\sigma_i^A+\sum_j S_j^B\right), \quad (1)$$

where $\langle ij\rangle$ indicates a summation over all pair of nearest-neighboring sites, and H is an oscillating magnetic field of the form

$$H = H_0\cos(wt), \quad (2)$$

where H_0 and $w=2\pi\nu$ are the amplitude and the angular frequency of the oscillating field, respectively. The system is in contact with an isothermal heat bath at absolute temperature.

Now, we apply Glauber-type stochastic dynamics to obtain the mean-field dynamic equation of motion. Thus, the system evolves according to a Glauber-type stochastic process at a rate of $1/\tau$ transitions per unit time. Leaving the S spins fixed, we define $P^A(\sigma_1,\sigma_2,\ldots,\sigma_N;t)$ as the probability that the system has the σ-spin configuration, $\sigma_1,\sigma_2,\ldots,\sigma_N$, at time t, also, by leaving the σ spins fixed, we define $P^B(S_1,S_2,\ldots,S_N;t)$ as the probability that the system has the S-spin configuration, $S_1,S_2,\ldots,S_N$, at time t. Then, we calculate $W_i^A(\sigma_i\to\sigma_i')$ and $W_j^B(S_j\to S_j')$, the probabilities per unit time that the ith σ spin changes from σ_i to σ_i' and the jth S spin changes from S_j to S_j', respectively.

The time dependence of this probability function is assumed to be governed by the master equation which describes the interaction between spins and heat bath and can be written as

$$\frac{d}{dt}P^A(\sigma_1,\sigma_2,\ldots,\sigma_N;t) = -\sum_i\left(\sum_{\sigma_i\neq\sigma_i'}W_i^A(\sigma_i\to\sigma_i')\right)\times P^A(\sigma_1,\sigma_2,\ldots,\sigma_i,\ldots\sigma_N;t) + \sum_i\left(\sum_{\sigma_i\neq\sigma_i'}W_i^A(\sigma_i'\to\sigma_i)\times P^A(\sigma_1,\sigma_2,\ldots,\sigma_i',\ldots\sigma_N;t)\right), \quad (3)$$

where $W_i^A(\sigma_i\to\sigma_i')$ is the probability per unit time that the ith spin changes from the value σ_i to σ_i'. Since the system is in contact with a heat bath at absolute temperature T_A, each spin can change from the value σ_i to σ_i' with the probability per unit time;

$$W_i^A(\sigma_i\to\sigma_i') = \frac{1}{\tau}\frac{\exp[-\beta\Delta E^A(\sigma_i\to\sigma_i')]}{\sum_{\sigma_i'}\exp[-\beta\Delta E^A(\sigma_i\to\sigma_i')]}, \quad (4)$$

where $\beta=1/k_BT_A$, k_B is the Boltzmann factor, $\Sigma_{\sigma_i'}$ is the sum over the three possible values of $\sigma_i'=\pm1$, 0, and

$$\Delta E^A(\sigma_i\to\sigma_i') = -(\sigma_i'-\sigma_i)\left(J\sum_j S_j^B+H\right)-[(\sigma_i')^2-(\sigma_i)^2]\times\left(3K\sum_j[(S_j^B)^2-5/4]+3D\right), \quad (5)$$

gives the change in the energy of the system when the σ_i-spin changes. The probabilities satisfy the detailed balance condition

$$\frac{W_i^A(\sigma_i\to\sigma_i')}{W_i^A(\sigma_i'\to\sigma_i)} = \frac{P_A(\sigma_1,\sigma_2,\ldots,\sigma_i',\ldots,\sigma_N)}{P_A(\sigma_1,\sigma_2,\ldots,\sigma_i,\ldots,\sigma_N)}, \quad (6)$$

and substituting the possible values of σ_i, we obtain

$$W_i^A(1\to0) = W_i^A(-1\to0) = \frac{1}{\tau}\frac{\exp(-\beta y)}{2\cosh(\beta x)+\exp(-\beta y)}, \quad (7a)$$

$$W_i^A(1\to-1) = W_i^A(0\to-1) = \frac{1}{\tau}\frac{\exp(-\beta x)}{2\cosh(\beta x)+\exp(-\beta y)}, \quad (7b)$$

$$W_i^A(0\to1) = W_i^A(-1\to1) = \frac{1}{\tau}\frac{\exp(\beta x)}{2\cosh(\beta x)+\exp(-\beta y)}, \quad (7c)$$

where $x=H+J\Sigma_jS_j$ and $y=3K\Sigma_j[(S_j)^2-5/4]+3D$. Notice that, since $W_i^A(\sigma_i\to\sigma_i')$ does not depend on the value σ_i, we can therefore write $W_i^A(\sigma_i\to\sigma_i')=W_i^A(\sigma_i')$, then the master equation becomes

$$\frac{d}{dt}P^A(\sigma_1,\sigma_2,\ldots,\sigma_N;t) = -\sum_i\left(\sum_{\sigma_i\neq\sigma_i'}W_i^A(\sigma_i')\right)\times P^A(\sigma_1,\sigma_2,\ldots,\sigma_i,\ldots,\sigma_N;t) + \sum_i\left(\sum_{\sigma_i\neq\sigma_i'}W_i^A(\sigma_i)\times P^A(\sigma_1,\sigma_2,\ldots,\sigma_i',\ldots,\sigma_N;t)\right). \quad (8)$$

Since the sum of the probabilities is normalized to one, by multiplying both sides of Eq. (8) by σ_k for m_A and $(3\sigma_k^2-2)$ for q_A and taking the average, we obtain

$$\tau\frac{d}{dt}\langle\sigma_k\rangle = -\langle\sigma_k\rangle+\left\langle\frac{2\sinh(\beta x)}{2\cosh(\beta x)+\exp(-\beta y)}\right\rangle, \quad (9)$$

$$\tau\frac{d}{dt}\langle3\sigma_k^2-2\rangle = -\langle3\sigma_k^2-2\rangle+1-\left\langle\frac{3\exp(-\beta y)}{2\cosh(\beta x)+\exp(-\beta y)}\right\rangle. \quad (10)$$

These dynamic equations can be written in terms of a mean-field approach and hence the set of the mean-field dynamical equations in the presence of a time-varying field are

$$\tau\frac{d}{dt}\langle\sigma\rangle = -\langle\sigma\rangle + \frac{2\sinh\beta[Jz\langle S_j^B\rangle + H_0\cos(wt)]}{2\cosh\beta[Jz\langle S_j^B\rangle + H_0\cos(wt)] + \exp[-3\beta(Kz\langle Q_j^B\rangle + D)]}, \tag{11}$$

$$\tau\frac{d}{dt}\langle 3\sigma^2 - 2\rangle = -\langle 3\sigma^2 - 2\rangle + 1 - \frac{3\exp[-3\beta(Kz\langle Q_j^B\rangle + D)]}{2\cosh\beta[Jz\langle S_j^B\rangle + H_0\cos(wt)] + \exp[-3\beta(Kz\langle Q_j^B\rangle + D)]}. \tag{12}$$

The system evolves according to the set of these coupled differential equations given by Eqs. (11) and (12). They can be written in the form

$$\Omega\frac{d}{d\xi}m_A = -m_A + \frac{2\sinh[(1/T)(m_B + h\cos\xi)]}{2\cosh[(1/T)(m_B + h\cos\xi)] + \exp[-3(kq_B + \mathscr{d})/T]}, \tag{13}$$

$$\Omega\frac{d}{d\xi}q_A = -q_A + 1 - \frac{3\exp[-3(kq_B + \mathscr{d})/T]}{2\cosh[(1/T)(m_B + h\cos\xi)] + \exp[-3(kq_B + \mathscr{d})/T]}, \tag{14}$$

where $m_A=\langle\sigma\rangle$, $m_B=\langle S\rangle$, $q_A\equiv\langle 3\sigma^2-2\rangle$, $q_B\equiv\langle S^2\rangle-5/4$, $\xi=wt$, $T=(\beta zJ)^{-1}$, $h=H_0/zJ$, $k=K/zJ$, $\mathscr{d}=D/zJ$, and $\Omega=\tau w$.

Now assuming that the spins on sublattice A remain momentarily fixed and the spins on the sublattice B change, we obtain the mean-field dynamical equations of m_B and q_B for the B sublattice with the similar calculation as before, except we take $S_i=\pm 3/2, \pm 1/2$ instead of $\sigma_i=\pm 1, 0$ and we use $\langle q_B\rangle=\langle S_i^2-5/4\rangle$ instead of $\langle q_A\rangle=\langle 3\sigma_i^2-2\rangle$. The set of mean-field dynamical equations for the B lattice are obtained as

$$\Omega\frac{d}{d\xi}m_B = -m_B + \frac{3\sinh\left(\frac{3}{2}\frac{m_A + h\cos\xi}{T}\right)\exp\left[\frac{\mathscr{d} + kq_A}{T}\right] + \sinh\left(\frac{1}{2}\frac{m_A + h\cos\xi}{T}\right)\exp\left[-\frac{\mathscr{d} + kq_A}{T}\right]}{2\cosh\left(\frac{3}{2}\frac{m_A + h\cos\xi}{T}\right)\exp\left[\frac{\mathscr{d} + kq_A}{T}\right] + \cosh\left(\frac{1}{2}\frac{m_A + h\cos\xi}{T}\right)\exp\left[-\frac{\mathscr{d} + kq_A}{T}\right]}, \tag{15}$$

$$\Omega\frac{d}{d\xi}q_B = -q_B + \frac{\cosh\left(\frac{3}{2}\frac{m_A + h\cos\xi}{T}\right)\exp\left[\frac{\mathscr{d} + kq_A}{T}\right] - \cosh\left(\frac{1}{2}\frac{m_A + h\cos\xi}{T}\right)\exp\left[-\frac{\mathscr{d} + kq_A}{T}\right]}{\cosh\left(\frac{3}{2}\frac{m_A + h\cos\xi}{T}\right)\exp\left[\frac{\mathscr{d} + kq_A}{T}\right] + \cosh\left(\frac{1}{2}\frac{m_A + h\cos\xi}{T}\right)\exp\left[-\frac{\mathscr{d} + kq_A}{T}\right]}, \tag{16}$$

where $m_A=\langle\sigma\rangle$, $m_B=\langle S\rangle$, $q_A\equiv\langle 3\sigma^2-2\rangle$, $q_B\equiv\langle S^2\rangle-5/4$, $\xi=wt$, $T=(\beta zJ)^{-1}$, $h=H_0/zJ$, $k=K/zJ$, $\mathscr{d}=D/zJ$, and $\Omega=\tau w$. Hence, the set of mean-field dynamical equations of the system are obtained. We fixed $z=4$ and $\Omega=2\pi$. In the next section, we will give the numerical results of these equations.

III. NUMERICAL RESULTS AND DISCUSSIONS

A. Time variations of average order parameters

In order to investigate the behaviors of time variations of order parameters, first we have to study the stationary solutions of the set of coupled mean-field dynamical equations, given in Eqs. (13)–(16), when the parameters T, k, $\mathscr{d}$, and h are varied. The stationary solutions of these equations will be periodic functions of ξ with period 2π; that is,

$$m_A(\xi + 2\pi) = m_A(\xi) \quad \text{and} \quad m_B(\xi + 2\pi) = m_B(\xi), \tag{17a}$$

$$q_A(\xi + 2\pi) = q_A(\xi) \quad \text{and} \quad q_B(\xi + 2\pi) = q_B(\xi). \tag{17b}$$

Moreover, they can be one of three types according to whether they have or do not have the property

$$m_A(\xi + \pi) = -m_A(\xi) \quad \text{and} \quad m_B(\xi + \pi) = -m_B(\xi), \tag{18a}$$

$$q_A(\xi + \pi) = -q_A(\xi) \quad \text{and} \quad q_B(\xi + \pi) = -q_B(\xi). \tag{18b}$$

The first type of solution satisfies both Eqs. (18a) and (18b) is called a symmetric solution which corresponds to a disordered (d) solution. In this solution, the submagnetizations m_A and m_B are equal to each other ($m_A=m_B$), and they oscillate around zero and are delayed with respect to the external magnetic field. On the other hand, the quadrupolar order parameters $q_A(\xi)$ and $q_B(\xi)$ oscillate around a nonzero value for finite temperature and around zero for infinite temperature since $q_A=q_B=0$ at infinite temperature by the definition of $q_A=3\langle\sigma_i^2\rangle-2$ and $q_B=\langle S_j^2\rangle-5/4$, respectively. The second type of solution, that does not satisfy Eqs. (18a) and (18b), is also called a nonsymmetric solution but this solution corresponds to a ferrimagnetic (i) solution because the submagnetizations m_A and m_B are not equal each other ($m_A\neq m_B$), and

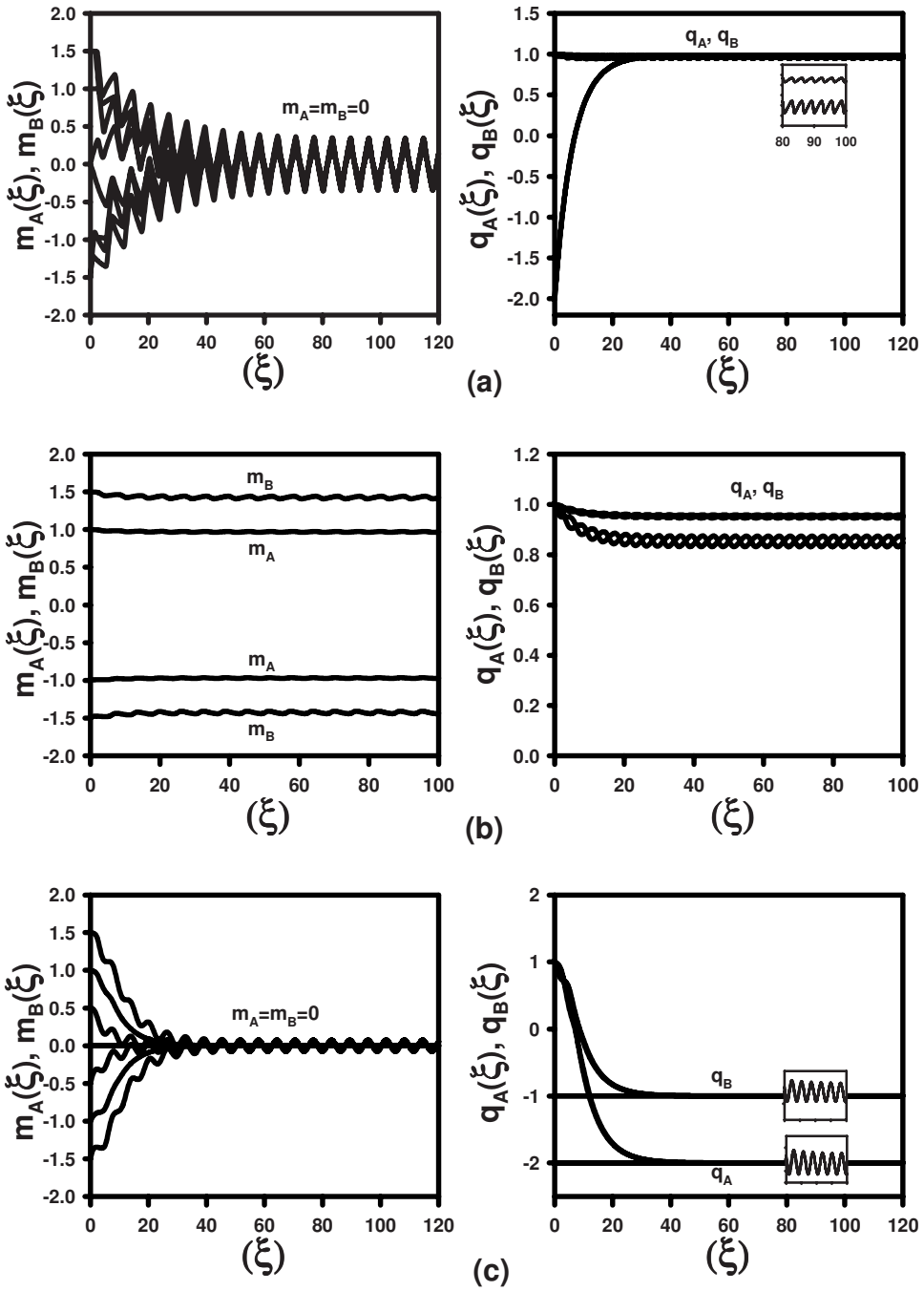

FIG. 1. Time variations of the magnetizations (m_A, m_B) and the quadrupole moments (q_A, q_B): (a) Exhibiting a disordered (d) phase: $k=0$, $\measuredangle=0.25$, $h=1.25$, and $T=0.25$. (b) Exhibiting a ferrimagnetic (i) phase: $k=0$, $\measuredangle=0.25$, $h=0.5$, and $T=0.5$. (c) Exhibiting an antiquadrupolar or staggered (a) phase: $k=0.25$, $\measuredangle=-1.0$, $h=0.75$, and $T=0.75$.

they oscillate around a nonzero value, namely, $m_A(\xi)$ and $m_B(\xi)$ oscillate around ± 1 and $\pm 3/2$, respectively. On the other hand, the quadrupolar order parameters q_A and q_B are not equal to each other $(q_A \neq q_B)$, and they oscillate around a nonzero value. In this case, the magnetization and quadrupolar order parameters do not follow the external magnetic field. The third type of solution, which satisfies Eq. (18a) but does not satisfy Eq. (18b), corresponds to the antiquadrupolar or staggered solution (a). In this solution, submagnetizations m_A and m_B are equal each other $(m_A=m_B)$, and $m_A(\xi)$ and $m_B(\xi)$ oscillate around zero value and are delayed respect the external magnetic field. On the other hand, the quadrupolar order parameters q_A and q_B are not equal to each other $(q_A \neq q_B)$, and they oscillate around a nonzero value, namely, $q_A(\xi)$ and $q_B(\xi)$ oscillate around -2 and -1, respectively, and they do not follow the external magnetic field. These facts are seen explicitly by solving Eqs. (13)–(16) numerically. These equations are solved by using the numerical Adams-Moulton predictor-corrector method for a given set of parameters and initial values and presented in Fig. 1. Figures 1(a)–1(c) represent the disordered, ferromagnetic, and antiquadrupolar fundamental solutions or phases, respectively. In addition to these fundamental phases, four coexistence or mixed phases, namely, $i+d$, $i+a$, $a+d$, and $i+a+d$ mixed phases, occur in the system. The basic properties of the fundamental and mixed phases or solutions are summarized in Table I to avoid giving an unacceptable number of figures and as well as duplications of the explanations.

TABLE I. Characteristic of time variations of magnetizations $[m_A(\xi)$ and $m_B(\xi)]$ and quadrupolar order parameters $[q_A(\xi)$ and $q_B(\xi)]$.

			Oscillation of sublattice magnetization	Oscillation of sublattice quadrupole
Fundamental phases or solutions	d		$m_A=m_B=0$	$q_A \neq q_B>0$
	i		$m_A=\pm 1, m_B=\pm 3/2$	$q_A \neq q_B \neq 0$
	a		$m_A=m_B=0$	$q_A \neq q_B<0$
Coexistence phases or solutions	$i+d$	i	$m_A=\pm 1, m_B=\pm 3/2$	$q_A \neq q_B \neq 0$
		d	$m_A=m_B=0$	$q_A \neq q_B>0$
	$i+a$	i	$m_A=\pm 1, m_B=\pm 3/2$	$q_A \neq q_B \neq 0$
		a	$m_A=m_B=0$	$q_A \neq q_B<0$
	$a+d$	a	$m_A=m_B=0$	$q_A \neq q_B<0$
		d	$m_A=m_B=0$	$q_A \neq q_B>0$
	$i+a+d$	i	$m_A=\pm 1, m_B=\pm 3/2$	$q_A \neq q_B \neq 0$
		a	$m_A=m_B=0$	$q_A \neq q_B<0$
		d	$m_A=m_B=0$	$q_A \neq q_B>0$

B. Thermal behavior of dynamic order parameters

In this section, we investigate the behavior of the average order parameters in a period or the dynamic order parameters as a function of the reduced temperature. This investigation leads us to obtain the dynamic phase transition (DPT) points. The dynamic order parameters, namely, dynamic sublattice magnetizations (M_A, M_B) and dynamic sublattice quadrupole moments (Q_A, Q_B), are defined as

$$M_A = \frac{1}{2\pi}\int_0^{2\pi} m_A(\xi)d\xi, \quad M_B = \frac{1}{2\pi}\int_0^{2\pi} m_B(\xi)d\xi \quad (19)$$

and

$$Q_A = \frac{1}{2\pi}\int_0^{2\pi} q_A(\xi)d\xi, \quad Q_B = \frac{1}{2\pi}\int_0^{2\pi} q_B(\xi)d\xi. \quad (20)$$

The behaviors of M_A, M_B and Q_A, Q_B as a function of the reduced temperature for several values of k, $\measuredangle$, and h are obtained by solving Eqs. (19) and (20). We solve these equations by combining the numerical methods of Adams-Moulton predictor corrector with the Romberg integration. A few interesting results are plotted in Figs. 2(a)–2(e) in order to illustrate the calculation of the DPT points. In these figures, thick lines represent M_A and M_B, and thin line represents Q_A and Q_B. T_C and T_t represent second- and first-order phase transition temperatures, respectively. T_{tQ} is the first-order phase transitions for only Q_A and Q_B. Figure 2(a) shows the behavior of M_A, M_B and Q_A, Q_B as a function of the reduced temperature for $k=0$, $\measuredangle=0.25$, and $h=0.25$. In this figure, $M_A=1$, $M_B=3/2$, $Q_A=Q_B=1$ at zero temperature, and M_A and M_B decrease to zero continuously as the reduced temperature increases, therefore a second-order phase transition occurs at $T_C=1.1750$. On the other hand, Q_A and Q_B decrease until T_C, and it makes a cusp at T_C and then again decreases to zero as the reduced temperature increases, and finally it becomes zero at infinite temperature. In this case the dynamic phase transition is from the ferrimagnetic (i) phase to the d phase and the solution does not depend on initial values of M_A, M_B and Q_A, Q_B. Figures 2(b) and 2(c) illustrate the thermal variations of M_A, M_B and Q_A, Q_B for $k=0$, $\measuredangle=-0.3$, and $h=0.0625$ for two different initial values; i.e., the initial values are taken as $M_A=1$, $M_B=3/2$, and $Q_A=Q_B=1$ for Fig. 2(b) and $M_A=0$, $M_B=1/2$, $Q_A=-2$, and $Q_B=-1$ for Fig. 2(c). The behavior of Fig. 2(b) is similar to Fig. 2(a), hence the system undergoes a second-order phase transition from the i phase to the d phase. In Fig. 2(c), $M_A=0$, $M_B=0$ and $Q_A=-2$, $Q_B=-1$ at zero temperature, the system undergoes two successive phase transition as the temperature increases: The first one is a first-order phase transition, because discontinuously occurs for the dynamic order parameters. The transition is from the a phase to the i phase at $T_{tQ}=0.3150$. The second one is a second-order phase transition from the i phase to the d phase similar to Figs. 2(a) and 2(b). From Figs. 2(b) and 2(c), one can see that we have the $i+a$ coexistence phase region also exists in the system, compare Figs. 2(b) and 2(c), with Fig. 3(h). Figures 2(d) and 2(e) show the behavior of order parameters as a function of the reduced temperature for $k=0$, $\measuredangle=0.25$, and $h=1$ for two different initial values; i.e., the initial values are taken as $M_A=1$, $M_B=3/2$, and $Q_A=Q_B=1$ for Fig. 2(d) and $M_A=0$, $M_B=1/2$ and $Q_A=-2$, $Q_B=-1$ for Fig. 2(e). In Fig. 2(d), the system undergoes a first-order phase transition, because order parameters decrease to zero discontinuously as the reduced temperature increases and the phase transition is from the i phase to the d phase at $T_t=0.2350$. Figure 2(e) shows that $M_A=0$, $M_B=0$ and $Q_A=1$, $Q_B=1$ at zero temperature but does not undergo any phase transition and finally Q_A and Q_B become zero at infinite temperature; hence this figure corresponds to the d phase. From Figs. 2(d) and 2(e), one can see

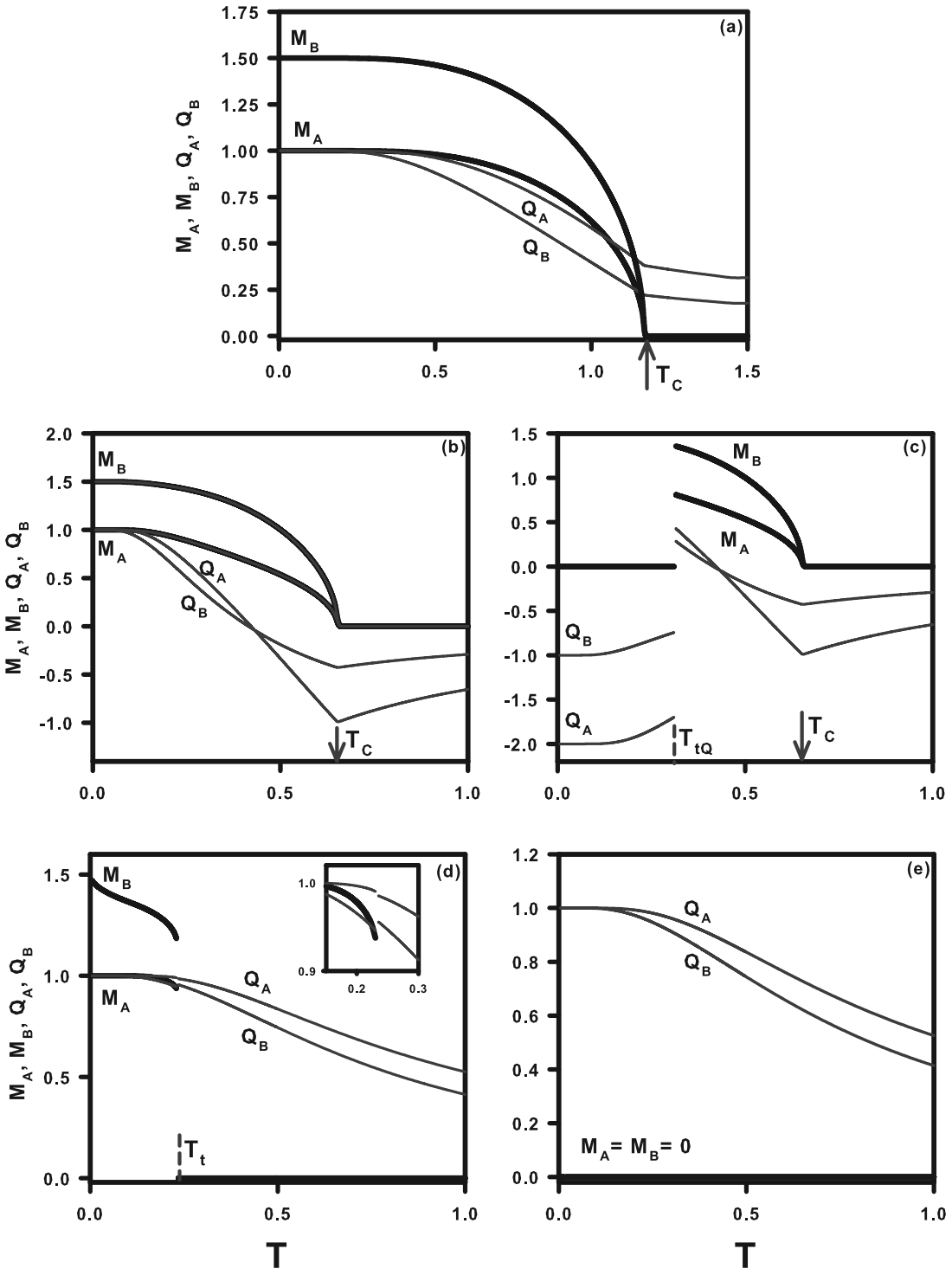

FIG. 2. The reduced temperature dependence of the dynamic magnetizations M_A and M_B (the thick solid lines) and the dynamic quadrupole moments Q_A and Q_B (the thin solid lines). T_C, and T_t are the critical or the second-order phase transition and the first-order phase transition temperatures for M_A, M_B, Q_A, and Q_B, respectively, and T_{tQ} is the first-order phase transition temperature for only Q_A and Q_B. (a) Exhibiting a second-order phase transition from the i phase to the d phase for $k=0$, $\diagup=0.25$, $h=0.25$, and the initial values of $M_A=1$, $M_B=3/2$ and $Q_A=1$, $Q_B=1$; 1.1750 is found as T_C. (b) Exhibiting a second-order phase transition from the i phase to the d phase for $k=0$, $\diagup=-0.3$, $h=0.0625$, and the initial values of $M_A=1$, $M_B=3/2$ and $Q_A=1$, $Q_B=1$; 0.6625 is found as T_C. (c) Exhibiting two successive phase transition, the first one is a first-order phase transition from the a phase to the i phase and the second one is a second-order phase transition from the i phase to the d phase for $k=0$, $\diagup=-0.3$, $h=0.0625$, and the initial values of $M_A=0$, $M_B=1/2$ and $Q_A=-2$, $Q_B=-1$; 0.3150 and 0.6625 are found as T_{tQ} and T_C, respectively. (d) Exhibiting a first-order phase transition from the i phase to the d phase for $k=0$, $\diagup=0.25$, $h=1.0$, and the initial values of $M_A=1$, $M_B=3/2$ and $Q_A=1$, $Q_B=1$; 0.2350 is found as T_t. (e) The system does not undergo any phase transition for $k=0$, $\diagup=0.25$, $h=1.0$, and the initial values of $M_A=0$, $M_B=1/2$ and $Q_A=-2$, $Q_B=-1$. This figure corresponds to d phase.

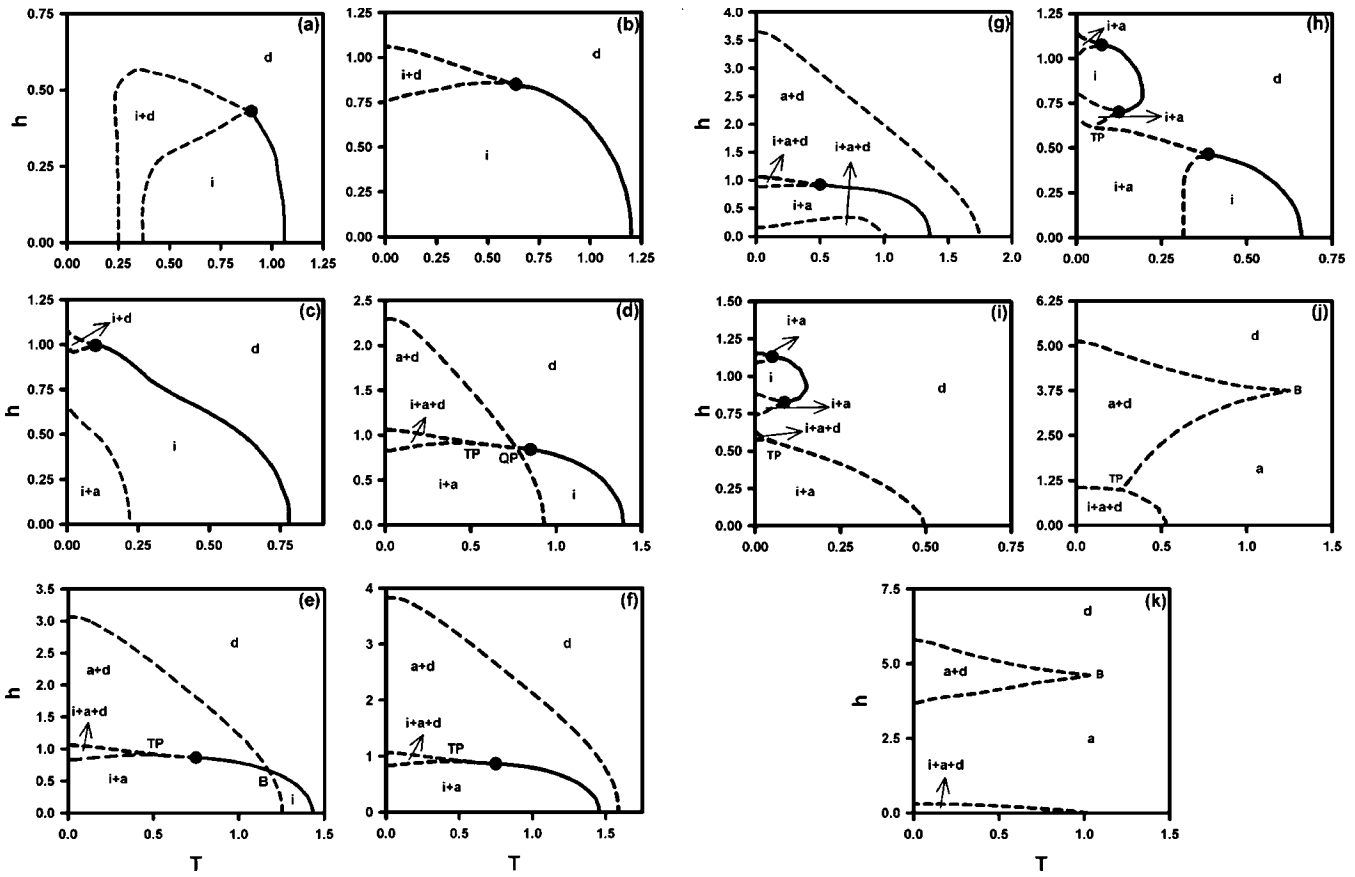

FIG. 3. Phase diagrams of the mixed spin-1 and spin-3/2 Ising ferrimagnetic model in the (h,T) plane. The disordered (d), ferrimagnetic (i), antiquadrupolar or staggered (a) phase and four different coexistence regions, namely, the $i+d$, $a+d$, $i+a$, and $i+a+d$ regions, are found. Dashed and solid lines represent the first- and second-order phase transitions, respectively. The special points are the dynamic tricritical point with filled circle, the dynamic double critical end point (B), dynamic triple point (TP), and dynamic quadruple point (QP). (a) $k=-0.135$, $\mathscr{A}=0$, (b) $k=0$, $\mathscr{A}=0.25$, (c) $k=0$, $\mathscr{A}=-0.25$, (d) $k=0.25$, $\mathscr{A}=0.25$, (e) $k=0.3125$, $\mathscr{A}=0.25$, (f) $k=0.375$ $\mathscr{A}=0.25$, (g) $k=0.30$, $\mathscr{A}=0$, (h) $k=0$, $\mathscr{A}=-0.30$, (i) $k=0$, $\mathscr{A}=-0.325$, (j) $k=0.25$, $\mathscr{A}=-0.75$, (k) $k=0.25$, $\mathscr{A}=-1$.

that the system exhibits the $i+d$ coexistence phase region, compare Figs. 2(d) and 2(e), with Fig. 3(b).

C. Dynamic phase diagrams

Since we have obtained the DPT points in Sec. III B, we can now present the phase diagrams of the system. The calculated phase diagrams in the (T,h), (k,T), and $(\mathscr{A},T)$ planes are presented in Figs. 3–5, respectively for various values of interaction parameters. In these phase diagrams, the solid and dashed lines represent the second- and first-order phase transition lines, respectively, and the dynamic tricritical points is denoted by a filled circle. B, Z, TP, and QP represent the dynamic double critical end point, zero-temperature critical point, triple point and quadruple point, respectively.

Figure 3 illustrates the dynamic phase diagrams in the (T,h) plane for various values k and $\mathscr{A}$ and eleven main different topological types of phase diagrams are seen. From these phase diagrams the following four interesting phenomena have been observed. (1) The phase diagrams of Figs. 3(a)–3(g), Fig. 3(i), and Fig. 3(h) illustrate one, two, or three tricritical points, respectively, but Figs. 3(j) and 3(k) do not contain any tricritical point; hence in these figures all the dynamic phase lines are only first-order lines. (2) In Fig. 3(a), the system also exhibits a reentrant behavior, i.e., as the temperature is lowered, the system passes from the disordered (d) phase to the $i+d$ coexistence or mixed phase, and back to the d phase again for high values of h. For low values of h, as the temperature is lowered, the system passes from the disordered (d) phase to the i phase, and from the i phase to the $i+d$ phase, and finally back to the d phase again. (3) The dynamic double critical end point (B), that separates one phase region from the other phase region, appears in the phase diagrams of Figs. 3(e), 3(j), and 3(k). (4) Figure 3(d) exhibits a quadruple point (QP), and Figs. 3(d)–3(f), and 3(h)–3(j) display a triple point (TP). We do indeed observe a phase diagram of Fig. 3(b) very similar to that found in earlier studies of the kinetic spin-1/2 Ising model [16], the kinetic Blume-Capel (BC) model [17], Blume-Emery-Griffiths (BEG) model [18], the kinetic spin-3/2 Ising systems [19], as well as kinetics of the mixed spin-1/2 and spin-1 Ising ferrimagnetic system [6], but the phases other than the d phases are different. Moreover, a phase diagram similar to Fig. 3(c) has also been obtained in the kinetic BC [17], kinetic BEG [18], and kinetic isotropic BEG model [20], but the phases other than the d phases are different.

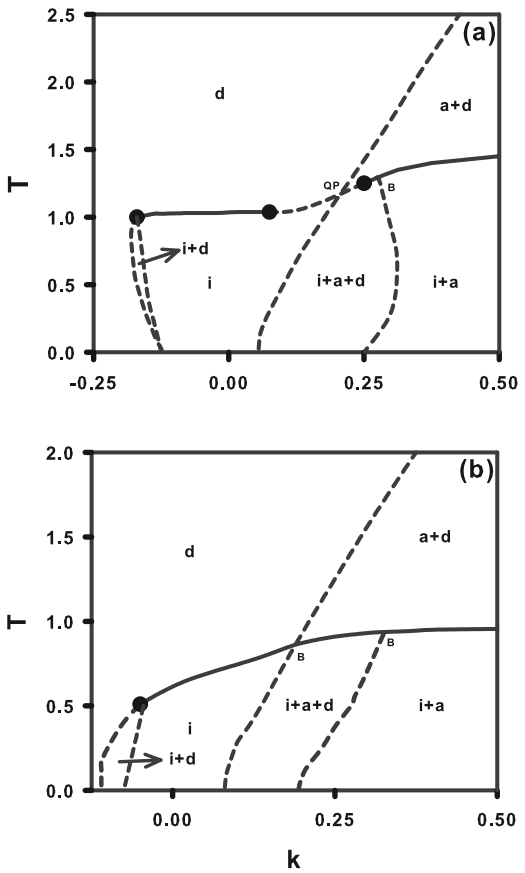

FIG. 4. Phase diagrams of the mixed spin-1 and spin-3/2 Ising ferrimagnetic model in the (k,T) plane. Dashed and solid lines are the dynamic first- and second-order phase boundaries, respectively; The special points are the dynamic tricritical point with filled circle, the dynamic double critical end point (B), and the dynamic quadruple point (QP). (a) $\mathscr{d}=0$, $h=0.25$, (b) $\mathscr{d}=0$, $h=0.8125$.

We also calculate the phase diagrams in the (k,T) and $(\mathscr{d},T)$ planes, seen in Figs. 4 and 5, respectively. We find seven different fundamental phase diagrams in the (k,T) plane and five main different topological types of phase diagrams in the $(\mathscr{d},T)$ plane. Since the phase diagrams in these planes can be readily obtained from the phase diagrams in the (T,h) plane, especially for very high and low values of h, we give two interesting phase diagrams in the (k,T) plane and one phase diagram in the $(\mathscr{d},T)$ plane in which they cannot readily be obtained from the phase diagrams in the (T,h) plane. Figures 4(a) and 4(b) illustrate the phase diagrams in the (k,T) plane. Figure 4(a) contains three dynamic tricritical points, one double critical end point (B), and one dynamic quadruple point (QP); the system also exhibits a reentrant behavior, same as seen in Fig. 3(a). In Fig. 4(b), one tricritical and two double critical end points (B) exists. One cannot easily obtain these properties from the phase diagrams in the (T,h) plane. Figure 5 contains one dynamic tricritical point and one zero-temperature critical point (Z) and again the occurrence of the Z point cannot be readily obtained from Fig. 3; however, if one examine very carefully Fig. 3, one can see the occurrence of the Z point. We have

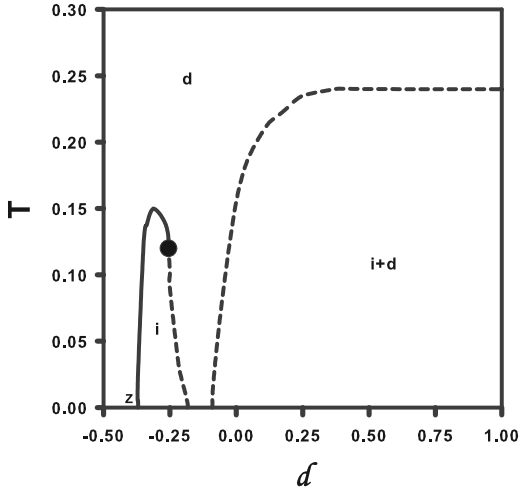

FIG. 5. Same as Fig. 4, but in the $(\mathscr{d},T)$ plane, obtained for $k=0$ and $h=1$. The special points are the dynamic tricritical point with filled circle and dynamic zero-temperature critical point (Z).

found a phase diagram similar to that obtained in the kinetic spin-1 Blume-Capel model in the $(\mathscr{d},T)$ plane very recently [21].

IV. SUMMARY AND CONCLUSION

We have analyzed, within a mean-field approach, the stationary states of the kinetic mixed spin-1 and spin-3/2 Ising ferrimagnetic model Hamiltonian with bilinear (J) and biquadratic (K) nearest-neighbor exchange interactions and a single-ion potential or crystal-field interaction (D) under the presence of a time varying (sinusoidal) magnetic field $[H=H_0\cos(wt)]$. We use a Glauber-type stochastic dynamics to describe the time evolution of the system. First we have studied time variations of the average order parameters in order to find the phases in the systems. Then, the behavior of the average order parameters in a period or the dynamic order parameters as a function of the reduced temperature $(T=kT/zJ$, z is the coordination number.) and a reduced crystal-field interaction $(\mathscr{d})$ is investigated. This study leads us to characterize the nature (continuous and discontinuous) of transitions as well as to obtain the DPT points. Finally, the dynamic phase diagrams are presented in the (T,h), (k,T), and $(\mathscr{d},T)$ planes, where $h=H_0/zJ$, $k=K/zJ$, and $\mathscr{d}=D/zJ$. We have found that the behavior of the system strongly depends on the values of the interaction parameters and eleven different phase diagram topologies are obtained in the (T,h) plane, seven different types of phase diagrams are found in the (k,T) plane, and five in the$(\mathscr{d},T)$. Since the phase diagrams in these planes can be readily obtained from the phase diagrams in the (T,h) plane, especially for very high and low values of h, we give two interesting phase diagrams in the (k,T) plane and one phase diagram in the $(\mathscr{d},T)$ plane in which they cannot be seen easily from the phase diagrams in the (T,h) plane. As explained in Sec. III C and seen in Figs. 3–5, the system displays very rich different types of phase diagrams.

Finally, it should be mentioned there is a strong possibility that at least some of the first-order transition lines and also dynamic tricritical points are very likely artifacts of the mean-field approach due to its limitations, such as the correlations of spin fluctuations have not been considered. However, this study suggests that the kinetic mixed spin-1 and spin-3/2 Ising ferrimagnetic model has an interesting dynamic behavior. Hence, we hope that our detailed theoretical investigation may stimulate further work to study the nonequilibrium or DPT in the mixed Ising model by using more accurate techniques such as kinetic Monte Carlo (MC) simulations or renormalization-group (RG) calculations.

ACKNOWLEDGMENTS

This work was supported by the Scientific and Technological Research Council of Turkey (TÜBİTAK) Grant No. 107T533 and Erciyes University Research Fund Grant No. FBA-06-01.

[1] X. M. Weng and Z. Y. Li, Phys. Rev. B **53**, 12142 (1996).
[2] T. Kaneyoshi, Phys. Rev. B **55**, 12497 (1997).
[3] E. Albayrak and M. Keskin, J. Magn. Magn. Mater. **261**, 196 (2003).
[4] K. Htoutou, A. Ainane, and M. Saber, J. Magn. Magn. Mater. **269**, 245 (2004).
[5] T. Kasama, Y. Muraoka, and T. Idogaki, Phys. Rev. B **73**, 214411 (2006).
[6] G. M. Buendía and E. Machado, Phys. Rev. E **58**, 1260 (1998).
[7] M. Godoy and W. Figueiredo, Phys. Rev. E **61**, 218 (2000); **65**, 026111 (2002); **66**, 036131 (2002).
[8] C. Ekiz and M. Keskin, Physica A **317**, 517 (2003).
[9] J. Liu, Q. Zhang, H. Yu, and F. Sun, J. Magn. Magn. Mater. **288**, 48 (2005).
[10] A. Bobák and, M. Jurčišin, Physica B **233**, 187 (1997); Phys. Status Solidi B **204**, 787 (1997); T. S. Liu, G. Z. Wei, and Z. H. Xin, J. Magn. Magn. Mater. **173**, 179 (1997); A. Bobák, Physica A **258**, 140 (1998); Z. H. Xin, G. Z. Wei, and T. S. Liu, J. Magn. Magn. Mater. **188**, 65 (1998); G. Z. Wei, Z. H. Xin, and J. Wei, *ibid.* **204**, 144 (1999); A. Bobák, Physica A **286**, 531 (2000); A. Bobák, O. F. Abubrig, and D. Horváth, J. Magn. Magn. Mater. **246**, 177 (2002); W. Jiang, G. Z. Wei, and Z. D. Zhang, Phys. Rev. B **68**, 134432 (2003).
[11] O. F. Abubring, D. Horváth, A. Bobák, and M. Jaščur, Physica A **296**, 437 (2001).
[12] J. W. Tucker, J. Magn. Magn. Mater. **237**, 215 (2001).
[13] Y. Nakamura and J. W. Tucker, IEEE Trans. Magn. **38**, 2406 (2002); G. Z. Wei, Q. Zhang, and Y. Gu, J. Magn. Magn. Mater. **301**, 245 (2006).
[14] E. Albayrak, Int. J. Mod. Phys. B **17**, 1087 (2003); E. Albayrak and A. Alçi, Physica A **345**, 48 (2005); C. Ekiz, J. Magn. Magn. Mater. **307**, 139 (2006).
[15] R. J. Glauber, J. Math. Phys. **4**, 294 (1963).
[16] T. Tomê and M. J. de Oliveira, Phys. Rev. A **41**, 4251 (1990).
[17] M. Keskin, O. Canko, and Ü. Temizer, Phys. Rev. E **72**, 036125 (2005).
[18] O. Canko, Ü. Temizer, and M. Keskin, Int. J. Mod. Phys. C **17**, 1717 (2006).
[19] M. Keskin, O. Canko, and B. Deviren, Phys. Rev. E **74**, 011110 (2006); O. Canko, B. Deviren, and M. Keskin, J. Phys.: Condens. Matter **118**, 6635 (2006); M. Keskin, O. Canko, and M. Kırak, J. Stat. Phys. **171**, 359 (2007).
[20] M. Keskin, O. Canko, and E. Kantar, Int. J. Mod. Phys. C **17**, 1239 (2006).
[21] M. Keskin, O. Canko, and Ü. Temizer, J. Exp. Theor. Phys. **104**, 936 (2007).